



HAL
open science

Sources of discrepancies between satellite-derived and land surface model estimates of latent heat fluxes

Alan Lipton, Pan Liang, Carlos Jiménez, Jean-Luc Moncet, Filipe Aires, Catherine Prigent, Richard Lynch, John Galantowicz, Robert d'Entremont, Gennady Uymin

► To cite this version:

Alan Lipton, Pan Liang, Carlos Jiménez, Jean-Luc Moncet, Filipe Aires, et al.. Sources of discrepancies between satellite-derived and land surface model estimates of latent heat fluxes. *Journal of Geophysical Research: Atmospheres*, 2015, 120 (6), pp.2325-2341. 10.1002/2014JD022641 . hal-02397855

HAL Id: hal-02397855

<https://hal.science/hal-02397855>

Submitted on 1 Jan 2022

HAL is a multi-disciplinary open access archive for the deposit and dissemination of scientific research documents, whether they are published or not. The documents may come from teaching and research institutions in France or abroad, or from public or private research centers.

L'archive ouverte pluridisciplinaire **HAL**, est destinée au dépôt et à la diffusion de documents scientifiques de niveau recherche, publiés ou non, émanant des établissements d'enseignement et de recherche français ou étrangers, des laboratoires publics ou privés.

Copyright

RESEARCH ARTICLE

10.1002/2014JD022641

Key Points:

- Satellite-model difference analysis identified model parameterization problems
- Satellite-model difference analysis identified problems with model precipitation
- Latent heat fluxes from satellite and upscaled flux tower data were similar

Correspondence to:

A. E. Lipton,
alipton@aer.com

Citation:

Lipton, A. E., P. Liang, C. Jiménez, J.-L. Moncet, F. Aires, C. Prigent, R. Lynch, J. F. Galantowicz, R. P. d'Entremont, and G. Uymin (2015), Sources of discrepancies between satellite-derived and land surface model estimates of latent heat fluxes, *J. Geophys. Res. Atmos.*, *120*, 2325–2341, doi:10.1002/2014JD022641.

Received 28 SEP 2014

Accepted 20 FEB 2015

Accepted article online 26 FEB 2015

Published online 26 MAR 2015

Sources of discrepancies between satellite-derived and land surface model estimates of latent heat fluxes

Alan E. Lipton¹, Pan Liang¹, Carlos Jiménez², Jean-Luc Moncet¹, Filipe Aires², Catherine Prigent^{2,3}, Richard Lynch¹, John F. Galantowicz¹, Robert P. d'Entremont¹, and Gennady Uymin¹

¹Atmospheric and Environmental Research, Inc., Lexington, Massachusetts, ²Estellus, Paris, France, ³CNRS, Laboratoire d'Etudes du Rayonnement et de la Matière en Astrophysique, Observatoire de Paris, Paris, France

Abstract Monthly-average estimates of latent heat flux have been derived from a combination of satellite-derived microwave emissivities, day-night differences in land surface temperature (from microwave AMSR-E), downward solar and infrared fluxes from ISCCP cloud analysis, and MODIS visible and near-infrared surface reflectances. The estimates, produced with a neural network, were compared with data from the Noah land surface model, as produced for GLDAS-2, and with two alternative estimates derived from different datasets and methods. Areas with extensive, persistent, substantial discrepancies between the satellite and land surface model fluxes have been analyzed with the aid of data from flux towers. The sources of discrepancies were found to include problems with the model surface roughness length and turbulent exchange coefficients for midlatitude cropland areas in summer, inaccuracies in the precipitation data that were used as forcing for the land surface model, and model underestimation of transpiration in some forests during dry periods. At the tower sites analyzed, agreement with tower data was generally closer for our satellite-derived fluxes than for the land surface model fluxes, in terms of monthly averages.

1. Introduction

Land surface fluxes of water mass and latent heat are among the highly uncertain components of the water and energy cycles, with substantial disagreement among fluxes estimated by land surface models and various types of retrievals from satellite and other data sets [Jiménez *et al.*, 2011; Vinukollu *et al.*, 2012; Peters-Lidard *et al.*, 2011]. No single data set or methodology has emerged as a standard for land flux estimation. The uncertainties among model results are of particular concern for addressing scientific questions for which reliable models are essential, including understanding water cycle processes and predicting water cycle aspects of global change. In contrast to the problem over ocean, the land flux process is complicated by biological processes of vegetation, terrain and landcover structure, and variable soil texture and moisture. From a global remote sensing standpoint, the difficulties over land are compounded by the fact that some key elements of flux processes (e.g., stomatal resistance and turbulent forcing by wind) are, at best, retrievable only with application of parameterizations that have large uncertainties. Nevertheless, visible, infrared, and microwave satellite data contain information about near-surface soil and vegetative properties that are strongly related to surface water and heat fluxes, but the relationships of the satellite measurements to surface water fluxes are indirect and incomplete.

Numerous methods have been developed for estimating land surface water fluxes using remote sensing data, as have been reviewed by Wang and Dickinson [2012] and others referenced therein. These methods rely, to varying degrees, on empirical relationships, energy balance constraints, and diagnostic models of physical processes related to surface fluxes. Most of these methods rely on products derived from visible and infrared satellite data, such as vegetation indices and land surface temperature, in combination with near-surface meteorological data from atmospheric data assimilation or other sources. Microwave data have been used in a relatively small number of methods [e.g., Miralles *et al.*, 2011; Sun *et al.*, 2012; Jiménez *et al.*, 2009]. Microwave data have the disadvantage of relatively coarse spatial resolution (~20 km at best) but have the advantage of being available in cloudy and clear areas, avoiding the biases of visible and infrared measurements toward clear-sky conditions.

Data assimilation systems are an attractive option for flux estimation because they have the potential to optimally account for the information content and the error characteristics of all the data sources, while imposing constraints associated with the relevant physical processes represented by a numerical model [Reichle *et al.*, 2002; Rodell *et al.*, 2004]. When satellite measurements are used for data assimilation, they can be introduced in the form of radiometric measurements or in the form of retrieved characteristics. Land data assimilation has thus far emphasized the latter approach [e.g., Berg *et al.*, 2003]. Assimilated parameters of particular relevance to evaporation include the radiative flux, surface temperature, and soil moisture [e.g., Rodell *et al.*, 2004; Bosilovich *et al.*, 2007; Reichle *et al.*, 2007]. The use of retrieved parameters is most appropriate when the relationship between the surface characteristics and the radiometric measurements is simple and direct, and is more problematic when there are multiple surface characteristics that can have ambiguous effects on the measurements. In the case of soil moisture, currently available measurement systems leave considerable ambiguity between effects of moisture and other variables. The retrieved moisture products thus rely heavily on assumed parameters. When those parameters disagree with the formulations in the assimilating land surface model (LSM), there may be substantial biases [Reichle *et al.*, 2004]. Biases can be empirically reduced to the point that useful assimilation occurs [Reichle *et al.*, 2007], but information can be corrupted in this process because there is no way to be sure the bias-adjusted moisture is consistent with the satellite measurements. A related problem is an insufficient dynamic response of a retrieval algorithm to changes in soil moisture [Reichle *et al.*, 2007], in which case there is information lost upstream of the assimilating system. Successful assimilation requires that the model parameterizations and variables are consistent not only with evapotranspiration processes but also with the related visible, infrared, and microwave radiative processes that produce the signals measurable by satellite instruments. When they are inconsistent, the satellite information is effectively rejected or misguides the analysis.

As a step toward improved capabilities for estimating fluxes by land data assimilation, this paper addresses the identification and understanding of situations where model-produced fluxes are inconsistent with satellite data products. In particular, we focus on seasonally persistent regional discrepancies. Such discrepancies may result from the model behavior being inconsistent with the actual behavior of surface properties represented in the satellite measurements, from shortcomings in the methodology used in satellite data processing, or from both.

The LSM considered here is the widely used Noah model [Ek, *et al.*, 2003]. The LSM latent heat fluxes were compared with fluxes retrieved from a combination of visible, infrared, and microwave satellite data, on monthly time scales, using a neural network similar to the one used by Jiménez *et al.* [2009]. For context, these fluxes are compared with two widely used flux estimates generated from satellite and other data sources. We then go beyond comparisons to investigate the sources of some discrepancies between the flux estimates, in instances where these discrepancies are prominent by their magnitude, their regional extent, and their persistence over at least 2 months. These regional discrepancy analyses incorporate time series of in situ data from flux towers. The discrepancy investigations presented here are restricted to instances for which flux tower data were available, due to the importance of the independent in situ data for drawing conclusions regarding the sources of discrepancies.

2. Methodology

2.1. Neural Network Approach

Neural network (NN) training for prediction of latent heat fluxes (LE) depends on matching the predictor data (section 2.2.1) with reference LE data, using a data set with a sufficient number and diversity of conditions for robust modeling of the statistical relationships. We required reference data that were largely independent of the satellite information sources being evaluated in this study. These criteria are not met by tower measurements or global flux analyses (section 2.2.4). Instead, we used LE data from the Noah LSM in the training. This approach has the weakness that the NN inherits global biases from the particular LSM and its skill is, to some degree, constrained by the accuracy of the LSM. The regional and temporal variability of the NN-derived LE is, however, determined entirely by the variability of the satellite-derived inputs, so these aspects of the NN-derived LE are not inherited from the LSM. This property follows from our approach of training the NN with a single pool of data covering all seasons, regions, and surface types, with no explicit

information about location or time among the NN inputs. The NN products can, therefore, provide a degree of independent skill, with the capability to detect potential problems in the LSM fluxes [Jiménez *et al.*, 2011].

2.2. Data Sources

2.2.1. Satellite Data

The selection of satellite data types to use in the flux estimation was based on the selection by Jiménez *et al.* [2009], while more recent data sources were used for some of the data. All of the selected data sets spanned the year 2003, which was the period of focus for this study.

Visible and near-infrared reflectances from the Moderate Resolution Imaging Spectroradiometer (MODIS) on the Aqua spacecraft were used primarily for their information regarding green vegetation. Specifically, we used surface reflectances in the blue, red, and near-infrared (bands 3, 1, and 2, respectively) that are intermediate products in generation of the Enhanced Vegetation Index (EVI) monthly 1 km data set (MYD13A3) [Huete *et al.*, 1999]. We used the individual reflectances to allow the nonlinear neural network access to the full information content of the channels rather than use data reduced to EVI.

Passive microwave surface emissivities from the Advanced Microwave Scanning Radiometer-EOS (AMSR-E) provide information regarding surface moisture and vegetative properties including the water content [Ferrazzoli *et al.*, 1992; Prigent *et al.*, 2001]. The emissivities were taken from the merged product of Moncet *et al.* [2011], which resulted from filtering and averaging over monthly intervals. These emissivities were produced on a fixed global sinusoidal grid with 27.8 km spacing, for vertical and horizontal polarizations at 10.65, 18.7, 36.5, and 89 GHz.

Land surface temperatures (LST) retrieved from AMSR-E data were included to represent the diurnal change in surface temperature, whose relationship to the partition of energy between latent and sensible heat fluxes has been exploited in satellite remote sensing of these fluxes [Diak, 1990; Wang *et al.*, 2006; Anderson *et al.*, 2007]. These and most other applications of LST for flux estimation have relied on infrared data sources [e.g., Price, 1980; Stisen, *et al.*, 2008; Venturini *et al.*, 2008; Lu and Zhuang, 2010; Tang *et al.*, 2010; Ryu *et al.*, 2011]. AMSR-E data cannot represent the full diurnal cycle because measurements were made just twice per day, according to the Aqua sun-synchronous orbit; however, the measurement times (01:30 and 13:30 local time) were suitable for approximating the diurnal range of LST. We retrieved LST from 10.65 GHz vertical-polarization brightness temperatures (T^B) by solving a simple form of the radiative transfer equation:

$$T^B = T^\uparrow + \tau[\varepsilon T_e + (1 - \varepsilon)T^\downarrow], \quad (1)$$

where T_e is the effective emitting temperature of the surface, τ is the total atmospheric transmittance along the sensor line of sight, T^\uparrow and T^\downarrow represent the upwelling and downwelling atmospheric emission, respectively, and ε is the surface emissivity [Moncet, *et al.*, 2011]. The retrievals of day (13:30) and night (01:30) LST were based on emissivities retrieved from separate day and night data. In applying this equation, we used T_e to represent the LST and we used emissivities derived at a monthly time scale with a nonpenetration approximation. For surfaces with significant penetration, these approximations introduce errors that offset each other to the extent that the day and night differences between the LST and T_e are each constant over the monthly period represented by the emissivities. Issues related to penetration are discussed more extensively by Galantowicz *et al.* [2011]. A radiative transfer model was used to compute τ , T^\uparrow , and T^\downarrow [Liebe *et al.*, 1992; Rosenkranz, 1998] with atmospheric data derived from the Global Data Assimilation System (GDAS) analysis [Kanamitsu, 1989; Kalnay *et al.*, 1990]. As input to the neural network, we used the day-night difference in LST (Δ LST).

The net radiative flux at the surface (R_n) can be viewed as the available energy source for the combination of latent, sensible, and ground heat fluxes [Wang and Dickinson, 2012]. While satellite-derived R_n products are available, they depend heavily on data from numerical models. We chose to avoid this influence of numerical models on our retrieved fluxes by using satellite-derived downward shortwave and longwave radiative fluxes as inputs to the neural network rather than R_n . The reflected (upward) shortwave radiation is indirectly and approximately represented by the MODIS reflectance data discussed above. In particular, we used radiative fluxes from the International Satellite Cloud Climatology Project (ISCCP) FD product [Zhang, *et al.*, 2004].

2.2.2. Land Surface Model Data

The LSM data against which we compared the satellite-derived products were taken from the Global Land Data Assimilation System 2 (GLDAS-2) [Rodell *et al.*, 2004]. The data available for the work reported

here were from Experiment 1, which used the Noah LSM (version 2.7.1) at 1° spatial resolution. More recently, subsequent versions of Noah and the GLDAS-2 experiments have been produced. Considering that LSMs and their input data are being constantly updated, our analyses of LSM data were not aimed at validation or development of this specific version but rather at understanding the behavior of this model in relation to the information from satellite data toward identifying factors that may present challenges to land data assimilation.

2.2.3. Flux Tower Data

Eddy covariance flux measurements and other relevant data were taken from several sites in the FLUXNET [Baldocchi, et al., 2001] and Ameriflux [Ocheltree and Loescher, 2007] networks. For Ameriflux sites, we used level-4 data, which are gap filled [Moffat et al., 2007]. Flux estimates from eddy covariance instruments are subject to several significant sources of error, including local heterogeneity and insensitivity to scales of motion that contribute to time-averaged fluxes, and which may result in the estimated components of the surface energy budget being unrealistically out of balance with each other [Baldocchi, 2003; Massman and Lee, 2002; Mauder and Foken, 2006; Mauder, et al. 2010]. When used as reference for analyzing flux data from satellites and LSMs [e.g., Fisher et al., 2008; Vinukollu et al., 2011], an additional hindrance is the scale discrepancy between the area represented by the tower measurements and the averaging area of the satellite and LSM gridded fields, the significance of which depends on the degree of surface heterogeneity at these scales [Li et al., 2008]. Despite these limitations, flux tower measurements are useful reference because they are independent of the satellite and LSM-based estimates. The availability of tower data at high time resolution (30 min) is valuable because it allows analysis of relationships among variables to provide insight into the processes affecting monthly and longer-term averages.

2.2.4. Other Flux Analyses

As additional points of reference for our satellite-derived fluxes and those from Noah, we considered widely used flux data from upscaled FLUXNET data and from the MODIS global terrestrial evapotranspiration product (MOD16). Both of these data sets are derived from a combination of surface-based and satellite-based measurements. The former data set was derived with a model tree ensemble (MTE) machine learning technique [Jung et al., 2011]. The upscaling incorporates 29 input variables to stratify environments and/or predict fluxes, including remotely sensed fraction of absorbed photosynthetically active radiation (PAR), and monthly and annual surface measurements. MOD16 fluxes are modeled based on the Penman-Monteith equation [Monteith, 1965] with inputs from daily meteorological data and MODIS land cover type, PAR, leaf area index, and albedo [Mu et al., 2011, 2013].

2.3. Neural Network Training

The architecture for the NN was a multilayer perceptron, with the satellite data as the first-level inputs and LE as the final output. The training data set was built from a sample of 100,000 data points, randomly selected from the data available in February, May, August, and November 2003, which prior work verified was sufficient to capture the annual variability [Jiménez et al., 2009]. The selection of data was equalized such that the training data set LE were uniformly distributed across the range of LE. Only points with valid data from all the observations and highest-quality AMSR-E emissivity data (according to the emissivity algorithm's quality criteria) were included in the training data set. Sites were excluded from the training and the analysis data sets where simple tests indicated likely snow cover or inundated land. After training, the NN was executed with data from each month of 2003.

Each of the satellite products were resampled to a 0.25° equal-area grid, except the ISCCP data that originated on that grid. The Noah data were produced on a 1° grid and were mapped to the 0.25° grid by selecting the nearest neighbor, so there would be a common grid for inputs and outputs of the NN training. The number of grid points with valid input data varied by month from 103,060 for January to 133,753 for September. The training data set was thus a small fraction of the domain (in space and time) over which the NN was applied.

3. Global Analyses

Some general characteristics of LE from each of the sources at global scales are evident in maps for July 2003 (Figure 1). Along with the broad similarities that follow the climate zones, there are substantial differences among the sources. The areas of highest LE are more spatially compact for Noah than for the

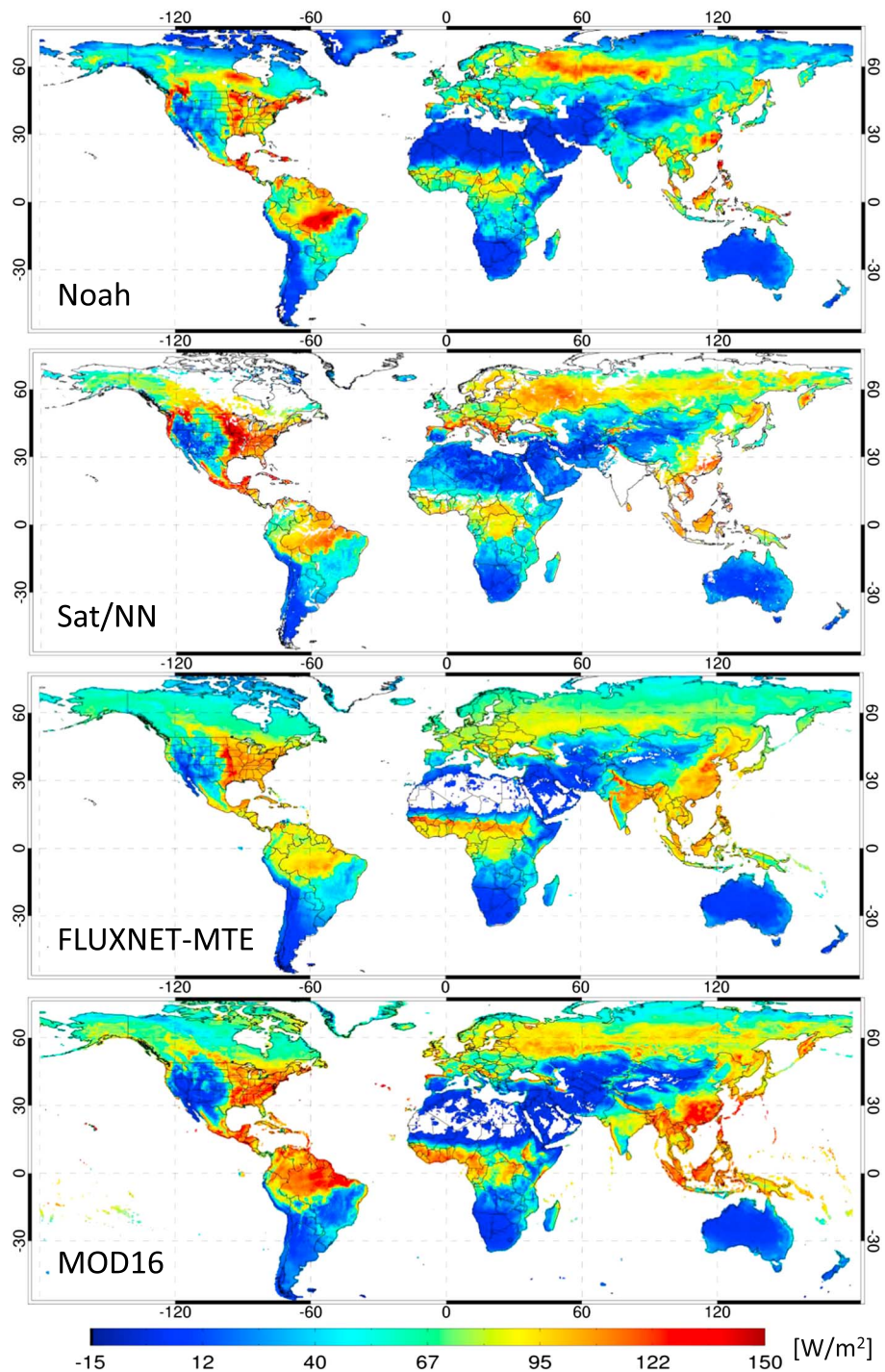


Figure 1. Latent heat fluxes for July 2003 from the data sources as labeled. Missing data over land (white) was, for the Sat/NN, mostly due to lack sufficient stable emissivity samples for monthly averaging (e.g., due to persistent cloud cover over India).

other sources, such as in northern Brazil and in North America. The LE from MOD16 differs substantially from both of the other products of remote sensing, particularly over South America, Africa, and southeastern Asia. The satellite/NN product has higher LE over much of southern Europe than the other products have. The satellite/NN LE differs less from the FLUXNET-MTE LE than from either Noah or MOD16 LE (14.4, 17.4, and 22.8 W/m² annual RMS, respectively). These relationships hold in every month, despite the facts that (1) the satellite/NN was trained using samples of these same Noah data and (2) the satellite/NN

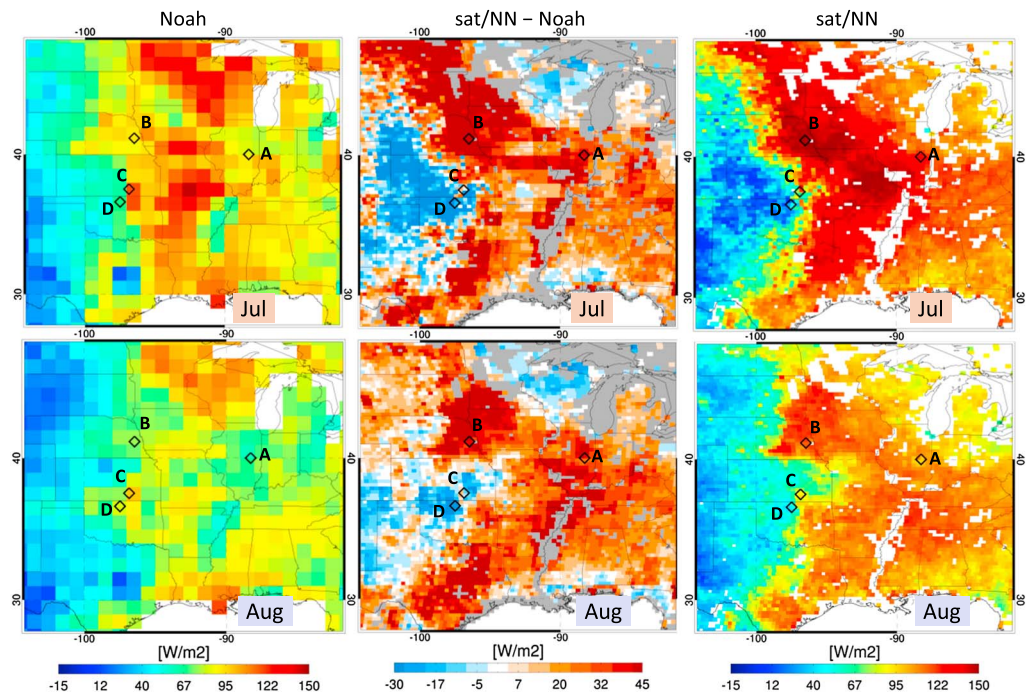


Figure 2. (left) LE from Noah, (right) the satellite/NN product, and the (middle) difference between the two for (top) July and (bottom) August. Instances where the satellite/NN LE is missing due to a missing NN input are gray in the difference plots and white in the satellite/NN plots. Selected flux tower sites are marked and labeled A–D.

and FLUXNET-MTE statistical methods use completely different inputs. These results indicate that the temporal and spatial features of the satellite/NN product are significantly independent from the Noah model. That independence, along with the relative consistency of the satellite/NN and FLUXNET-MTE, lends confidence in usefulness of satellite/NN LE for evaluating Noah model behavior.

4. Regional Analyses

4.1. Central Great Plains

There is a large, persistent discrepancy between Noah and satellite/NN LE over the Great Plains in the summer (Figure 2). The satellite/NN-derived LE has a pronounced gradient along the Great Plains in July, which weakens and becomes more locally concentrated in August. The Noah LE is similarly low in the west but has substantially different maxima toward the eastern plains. The largest differences are around the intersections of Nebraska, South Dakota, and Iowa in July.

The gradient in the satellite/NN LE generally follows a gradient in the green vegetation (EVI), and the microwave-derived Δ LST difference is also consistent with more diurnal surface heating and less latent heat flux to the west of the main LE gradient (Figure 3). These satellite products indicate high LE around the Nebraska / South Dakota / Iowa intersection, persisting from July to August, where the Noah LE is relatively low.

The analysis is supported by data from Ameriflux tower sites. Through July and August, the Nebraska site (in an irrigated corn field) [Suyker and Verma, 2009] has the highest LE among the tower sites in this region (Figure 4), with decreasing LE southward through the Kansas and Oklahoma sites. For these sites, the monthly-average satellite/NN LE for June–August generally agrees with the tower LE within 25 W/m^2 , with both indicating a strong drop in LE from the Nebraska site to the Oklahoma site. The Noah LE at these sites varies less than the other products from site-to-site and month-to-month, as the vegetative cycle evolves. These results are corroborated by analyses of the evaporative fraction (EF) over the July–August period (approximated as LE divided by the sum of LE and sensible heat flux, H), which is higher for the tower data than for Noah in Nebraska and is lower in Oklahoma, in each case by about a factor of 2 (not shown).

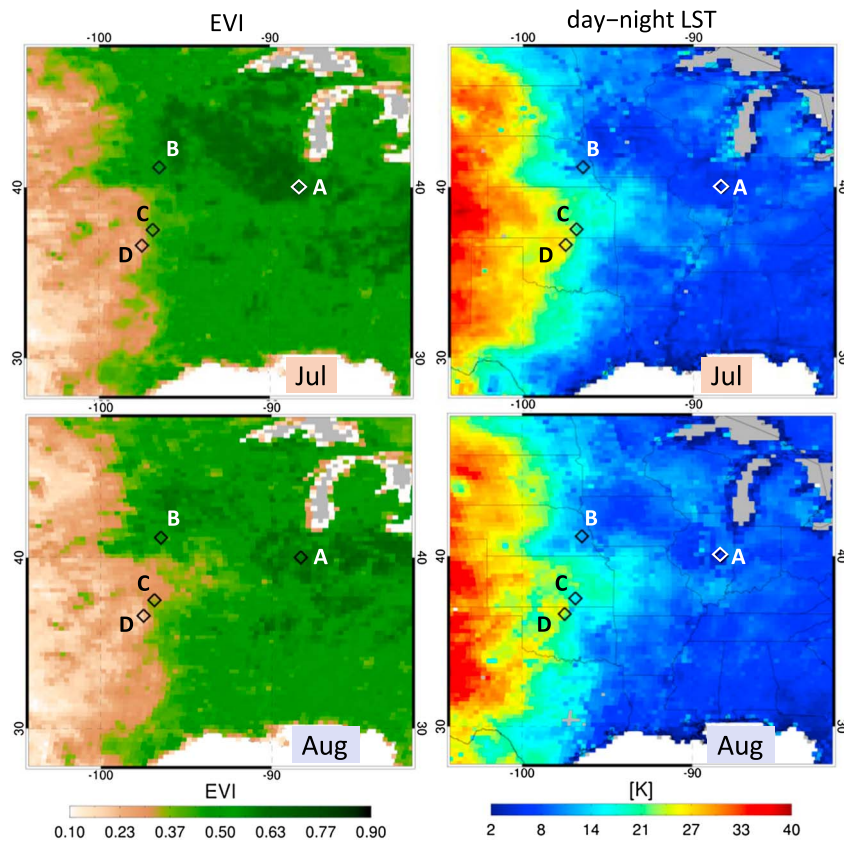


Figure 3. (left) Enhanced vegetation index (EVI) from MODIS and (right) day-night LST difference from AMSR-E for (top) July and (bottom) August.

A significant factor in the LE discrepancies is the band of relatively low Noah LE running from eastern South Dakota through Ohio and another in the central Mississippi River valley (Figure 2, top). This relatively low LE corresponds to low EF but is not associated with low soil moisture (Figures 5a and 5b). We found that the low Noah LE is related to the predominant landcover type (Figure 6). Comparing cropland to the surrounding landcover types, while excluding the arid grassland and scrubland areas to the west, the July LE is distinctly lower and satellite/NN–Noah LE discrepancies are distinctly higher for the areas classified as cropland. This relationship is not confined to the Great Plains area. The relationship is apparent when considering all of these land types in the 30°–60° band of the northern hemisphere (Figure 6). Frequency distributions of the discrepancies indicate that positive discrepancies are larger for croplands than for other landcover types throughout the summer in the central US, but only in July do croplands have a greatly different distribution than other landcover types (Figure 7). For the full 30°–60° band, only in July does the cropland distribution stand out from the others. Considering that (1) the discrepancies are highly distinct for cropland surface types, (2) the surface type classification is a Noah parameter that affects modeled fluxes, and (3) the satellite/NN products are derived without any regard to surface type classifications, these findings point to potential problems with the elements of the Noah parameterization dependent on the cropland type in this summer midlatitude environment.

In the configuration of Noah used for these runs, there are several parameters that depend on landcover type for the snow-free conditions relevant here. These parameters include the following:

1. The number of soil layers penetrated by roots has a direct effect on evapotranspiration (ET), which is closely related to LE, by way of the soil moisture volumetric content. Croplands have roots in three layers, versus four layers for the other landcover types represented in the eastern Great Plains. This difference is accounted for in the root-zone soil moisture plotted in Figure 5b, with the approximation that the root depth was taken as constant for the grid cell, while the Noah model treats fractional cover

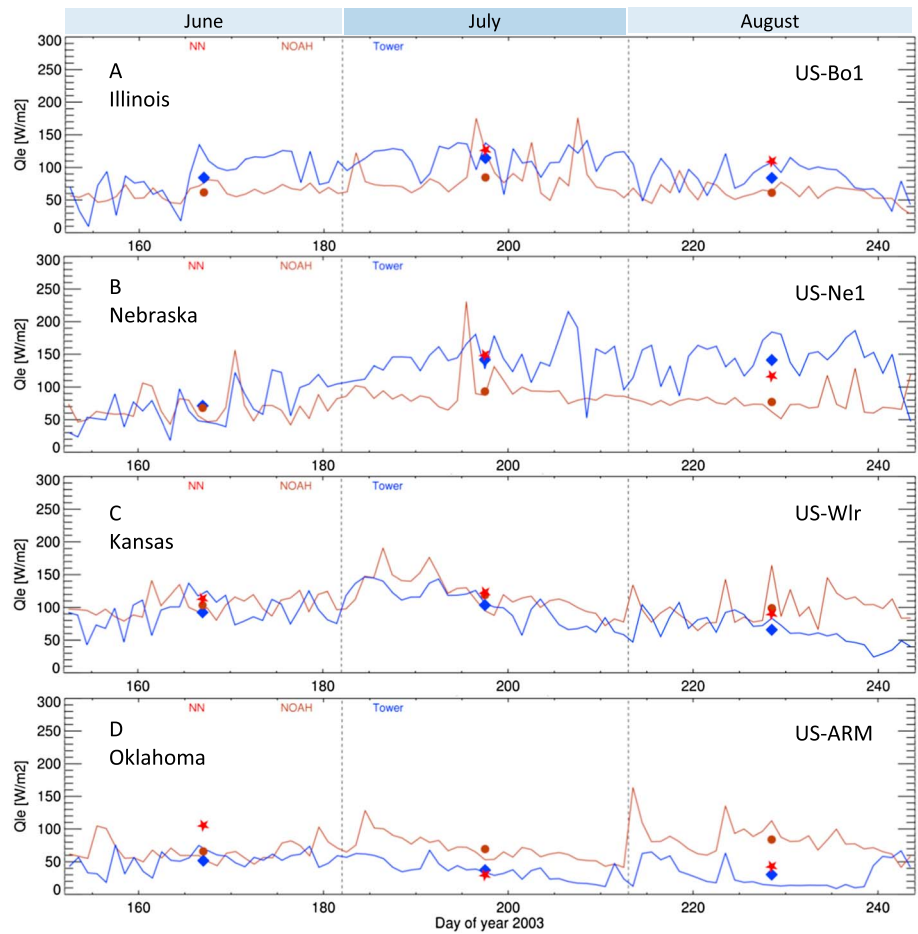
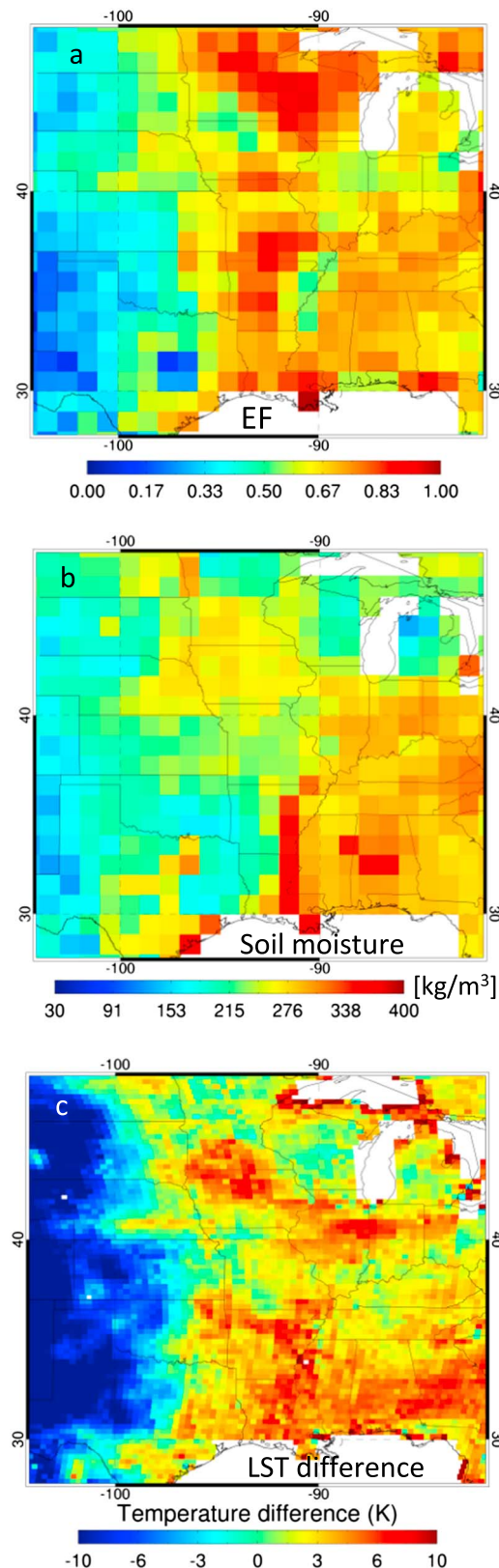


Figure 4. Daily-average LE from Noah (brown), the flux tower (blue), and the satellite/NN (red), for the sites marked A–D in Figure 2. The tower site identifiers are labeled at the right. The markers indicate the monthly averages.

of types during its integration. The root-zone soil moisture is relatively high in the relevant areas (discussed above) where the LE is relatively low, indicating that the root depth is not a driving factor in these features.

2. There are two parameters related to the stomatal resistance factor associated with solar radiation [Chen *et al.*, 1996]. We computed the net effect of these two parameters as a function of solar irradiance for each landcover type, while assuming there is no stress due to air temperature, vapor pressure deficit, or soil moisture availability. The net effect was for cropland to have lower resistance than any of the other types represented in the eastern Great Plains (Figures 6 and 7), indicating that these parameters were not driving factors in the low-LE features.
3. A parameter used to compute the stomatal resistance factor associated with the vapor pressure deficit is inversely related (by a series of equations) to ET. The cropland type has a lower value of this parameter than the other types represented in the eastern Great Plains, indicating that these parameters were not driving factors in the low-LE features.
4. The leaf area index (LAI) has a secondary dependence on landcover type, and a primary dependence on monthly maps of LAI, adjusted according to monthly maps of fractional green vegetation [Rodell *et al.*, 2004]. The primary effect of LAI on ET is a direct relationship, by way of the canopy resistance, and there is a secondary inverse influence via the radiation stress factor of the canopy resistance. The LAI is not relatively low in the areas that have relatively low LE running from eastern South Dakota through Ohio, nor is the fraction of green vegetation low in those areas (not shown). Both these parameters are relatively low in the central Mississippi river valley and thus contributed to the low LE and large discrepancies with the satellite/NN product in that area.



5. The roughness length (z_0) in Noah for cropland (0.035 m) is much lower than for the other, forested/wooded, types in the eastern Great Plains, by factors ranging from 16 to 31. The roughness length affects the surface exchange coefficient for heat and moisture through several terms, with a net direct relationship. As discussed by Mitchell *et al.* [2004, p. 23], a lower exchange coefficient would tend to lead to increased daytime surface temperature, decreased daytime available energy for evapotranspiration (the net radiation minus the heat flux into the soil), and decreased LE. The lower exchange coefficient, by itself, would also tend to reduce H, but an increased difference between the surface and air temperatures would have an opposite and partially compensating effect on H. The combined effects would tend to decrease EF. Figure 5c shows that Noah midday LST is indeed high relative to AMSR-E LST in these cropland areas with low LE. The relatively low Noah LST in relation to AMSR-E in arid areas toward the west is consistent with the findings of Zheng *et al.* [2012].

Beyond the Noah parameters controlled by the landcover type, the fraction of green vegetation also affects ET and LE, in a negative sense for direct evaporation from the soil, in a direct relationship with evaporation of canopy surface water (when wet), and in a direct relationship with potential transpiration. The net effect on ET would generally be direct, except possibly during short periods after rainfall when the soil surface is wet. As discussed in the context of its secondary influence on LAI, the values of this parameter in the low-LE areas that coincide with cropland are such that it would contribute to discrepancies in the central Mississippi river valley but not in the region from eastern South Dakota through Ohio.

Taken as a whole, the analyses discussed above give substantial evidence that the z_0 in cropland areas was too low during the summer growing season in these Noah runs, and the discrepancies with the satellite/NN LE in this region were

Figure 5. (a) July-average Noah evaporative fraction, (b) soil moisture volumetric content for the root zone, and (c) difference between Noah and AMSR-E midday (~13:30 local) LST. The soil moisture accounts for Noah's dependence of root zone depth on predominant land cover type.

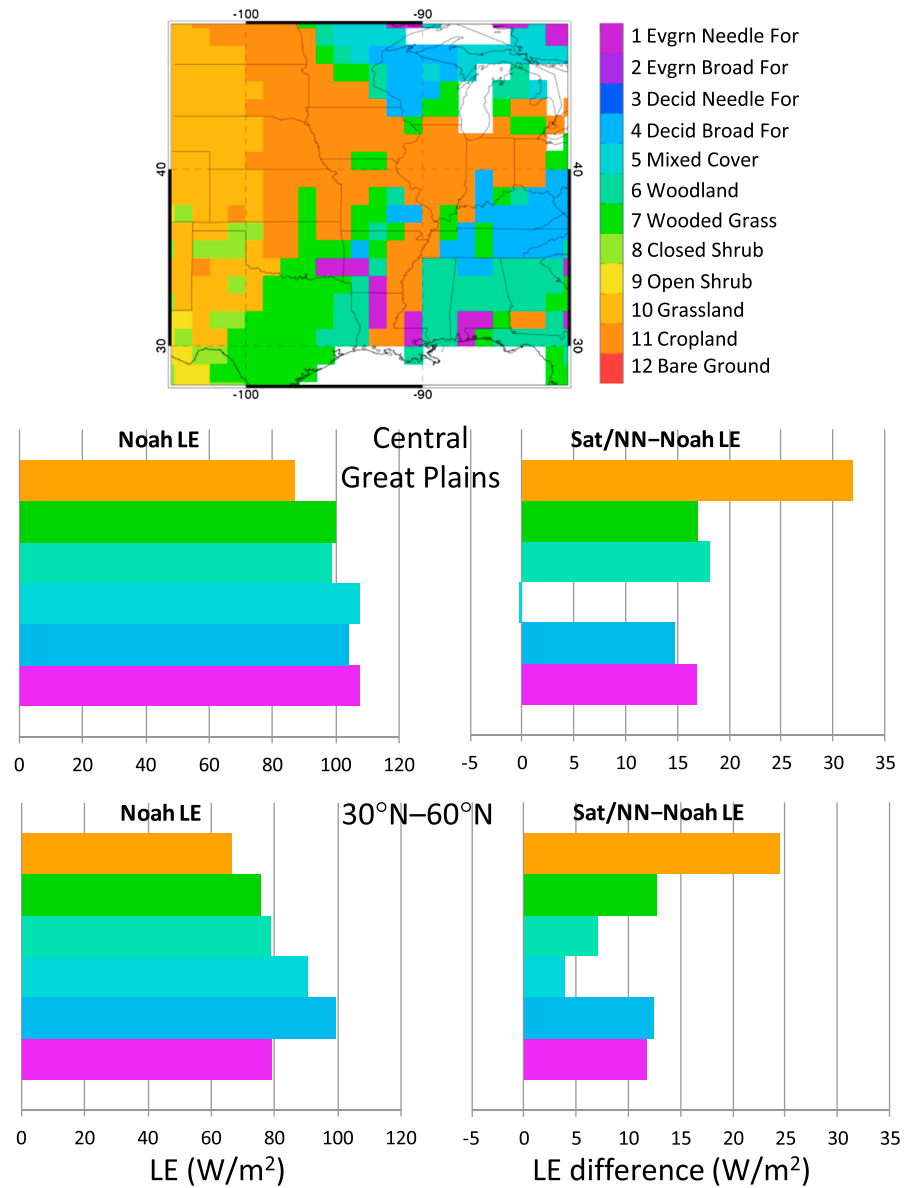


Figure 6. (top) Noah predominant landcover type and July-average values of Noah LE and satellite/NN–Noah LE, as labeled, (middle) for surface types in the central US, excluding the arid types of the western Great Plains, and (bottom) for the latitude band 30°N–60°N across all longitudes. The types are based on AVHRR data, as produced at the University of Maryland. Abbreviations are evgrn = evergreen, decid = deciduous, needle = needleleaf, broad = broadleaf, for = forest, grass = grassland, and shrub = shrubland.

largely attributable to this factor. Low LE in cropland areas of the Great Plains was evident also in summer season averages for years 2002–2008 for Noah v2.7.1 as configured for the North American Land Data Assimilation System (NLDAS), but they were not evident in NLDAS runs that used Noah v 3.2 [Peters-Lidard et al., 2011]. The consistency between our findings using GLDAS runs and the NLDAS findings using Noah v2.7.1 indicate that the features we analyzed are systematic features of this version of Noah parameterizations.

4.2. Northern California

In much of Northern and Central California, the discrepancies between satellite/NN and Noah LE were negative in the late spring and early summer and became positive from midsummer through the fall (Figure 8). These discrepancies covered portions of the Central Valley and the surrounding foothills and mountains.

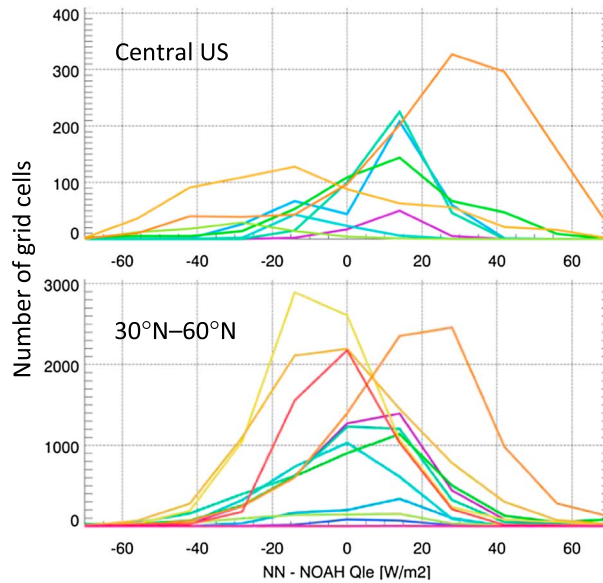


Figure 7. Frequency distribution of the number of grid cells as a function of the difference in LE between the satellite/NN and Noah products, for (top) the central US and (bottom) the latitude band 30°N–60°N for July 2003. The color scheme is as in Figure 6.

Over this period, flux tower data were available from Tonzi Ranch and Vaira Ranch Ameriflux sites (at 169 m and 133 m elevation, respectively). These sites are only 3 km apart in the Sierra Nevada foothills, but there are systematic differences between energy and water fluxes at the two sites related to differences in vegetation cover, with the Tonzi site classified as oak savanna woodland and the Vaira site as grassland [Baldocchi *et al.*, 2004]. A third site (Blodgett Forest) at higher (1280 m) elevation is in a ponderosa pine plantation, mixed-evergreen coniferous forest [Goldstein *et al.*, 2000]. The sloping terrain and variable vegetation cover accentuate the scale differences between the tower, satellite, and model data, but the discrepancies in LE are of sufficient magnitude and extent that the scale differences are not a major hindrance in this analysis.

The time series at Vaira and Tonzi are the same for the Noah and satellite/NN data because both sites are within a single grid box. The tower LE has a spring maximum at these sites and a secondary maximum in November (Figure 9). The early-summer drop in LE is sharper for Vaira than for Tonzi, where the predominant grasses at Vaira go dormant during the summer dry period while the scattered oak trees at Tonzi continue to transpire [Baldocchi *et al.*, 2004]. The Blodgett data indicate a summer maximum in LE associated with the maximum of net radiation in this heavily forested area (with correlation 89% for noon daily measurements over this 8-month period, in contrast to the 19% correlation at Vaira).

The Noah LE over these sites (which are all within a single grid box) responds strongly to the precipitation (Figure 10) and the corresponding surge in soil moisture and subsequent dry-down (not shown). In comparison with the tower data (which was similar at all 3 sites), the Noah precipitation is less frequent and more intense. The Noah model has major precipitation events in middle-late May, while the tower data indicate the spring precipitation season ending in early May. In relation to the precipitation, the Noah LE

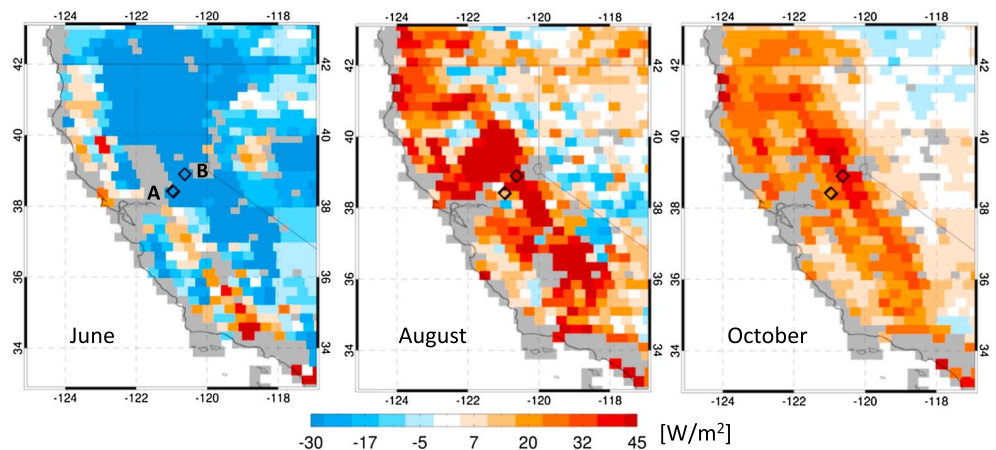


Figure 8. The difference in LE between the satellite/NN LE and the Noah LE for (left) June, (middle) August, and (right) October. The markers indicate the Tonzi Ranch and Vaira Ranch tower sites (A) and the Blodgett Forest site (B).

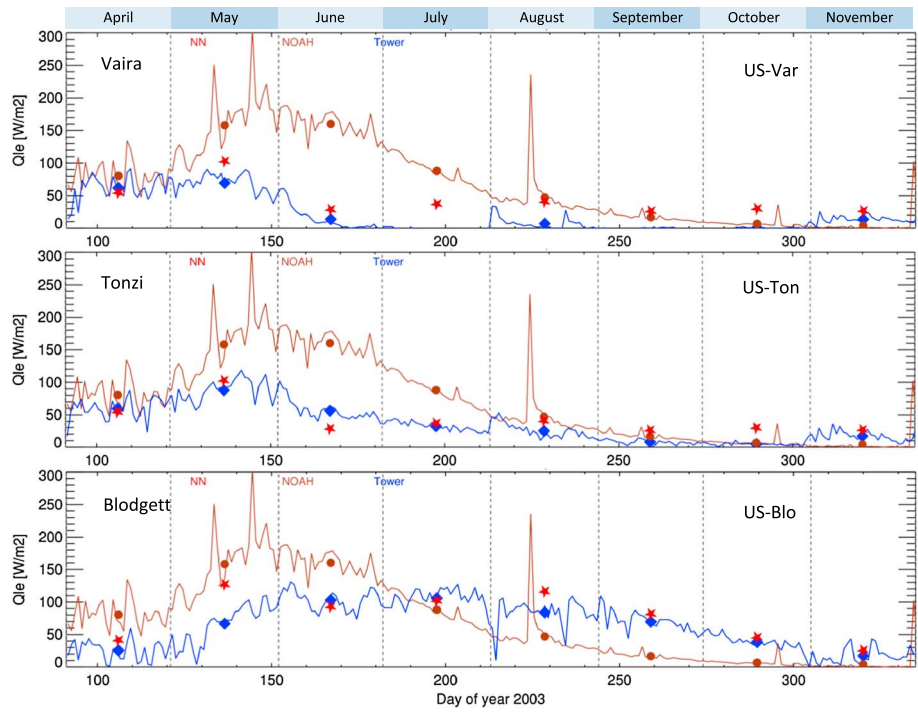


Figure 9. Daily-average LE from Noah (brown), the flux tower (blue), and the satellite/NN (red), for the Vaira, Tonzi, and Blodgett sites. The markers indicate the monthly averages.

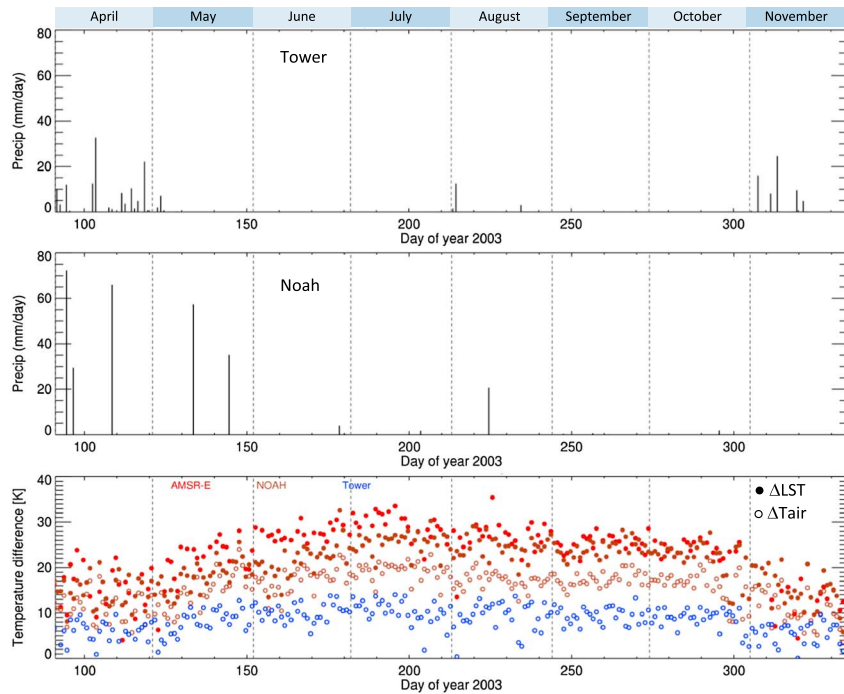


Figure 10. Daily precipitation at the Tonzi Ranch Ameriflux site from (top) the tower data and (middle) the Noah model, and (bottom) Δ LST (filled markers) and Δ Tair (unfiled markers). The temperature data sources are Noah (brown), the flux tower (blue), and AMSR-E (red).

continues to rise throughout May while the tower LE at Vaira and Tonzi begin to decrease by the end of the month. The tower data indicate substantial precipitation in November, with corresponding increases in LE, particularly at Vaira and Tonzi, while November precipitation in Noah was restricted to the end of the month and Noah LE was very low throughout the month. Precipitation is treated as an external forcing for Noah and, with this version of the GLDAS model, the precipitation data were from the Princeton data set [Sheffield *et al.* 2006], which merges data from several sources.

The monthly-average LE from the satellite/NN is generally within about 30 W/m^2 of averages from the tower data at these sites. These products agree with respect to the rise in LE from April to May and the drop in LE from May to June at Vaira and Tonzi but disagree significantly with respect to the May LE at Blodgett. At Vaira and Tonzi sites, the satellite/NN data lack the small rise in monthly-average LE in November. The satellite/NN data are consistent with the tower data with respect to the higher summer LE at Blodgett than at the other sites.

Time series of ΔLST and day-night air temperature differences (ΔTair) at Tonzi show the relationships between LE and the surface thermal diurnal cycle (Figure 10). In the tower data, ΔTair is highest in the June–October period, corresponding to the relatively low EF over that period. At the end of October the tower ΔTair decreases by about a factor of 2, corresponding to the onset of precipitation and the increase in LE, as would be expected with a shift from sensible heat to latent heat flux as moisture availability rises. The AMSR-E ΔLST (an input to the NN) follows a trend similar to the tower data and, as expected, the ΔLST is higher than the ΔTair . The ΔLST and the ΔTair vary less over this period for Noah than for the corresponding AMSR-E ΔLST and tower ΔTair . Statistically, the correlations with tower ΔTair are higher for AMSR-E ΔLST (83%) than for Noah ΔLST and ΔTair (both 58%), for the period covered by Figure 10. The May–July period when ΔLST is substantially higher for AMSR-E than for Noah corresponds to the period when the LE is substantially lower for the satellite/NN than for Noah.

It is apparent from these analyses that inaccuracies in the Noah precipitation forcing contributed to the LE discrepancies in this region over the summer and fall months. An additional factor in the discrepancies was the inability of the Noah model to represent the contribution of transpiration by trees toward elevating the LE in the summer dry season in the lower and upper mountain areas.

4.3. Southeast Australia

In Southeast Australia there were positive discrepancies between the satellite/NN and Noah LE in the January–April period, primarily in the coastal and near-coastal mountainous regions, with some negative discrepancies inland (Figure 11). The discrepancies were associated with relatively high satellite/NN LE in those coastal areas, with especially strong gradients in January. These features of the satellite/NN LE reflected corresponding gradients in the AMSR-E ΔLST that was among the inputs to the NN.

The Tumbarumba FLUXNET site [Leuning *et al.*, 2005; van Gorsel *et al.*, 2013] was located within the area of large January positive discrepancies. This site was in a broadleaf evergreen (*Eucalyptus*) forest. Due to large variations in vegetation, terrain, and other factors, we would not expect the controls on LE at this site to be representative of the entire area of positive discrepancies, but the site data are nevertheless useful for analyzing LE-related phenomena in a portion of that area.

According to the tower data, the LE decreased from month-to-month over the January–April period (Figure 12). The satellite/NN LE decreased similarly. The Noah LE was generally lower, particularly in January. The Noah LE surged with each precipitation event represented in the Noah forcing data (Figure 12), in accord with the simulated moistening and subsequent dry-down of the soil (not shown). The precipitation recorded at the tower site differed greatly from the Noah precipitation, and the tower LE tended to be lower during precipitation events than in surrounding periods (Figure 12). Over this period, the tower LE was highly correlated with the net radiation and the vapor pressure deficit (82% and 78%, respectively, for noon daily measurements), indicating that the amounts of available energy and atmospheric moisture (relative to a saturated surface) were primary factors in the LE variability. These correlations, along with the lack of tower LE response to precipitation (Figure 12), imply that soil moisture availability was not a primary factor in LE variability within this period. In the 2 months prior to January, there were 78 mm of precipitation accumulated over several events at the site, contributing to significant available water at the start of the analyzed period. The precipitation over late 2002 through early 2003 was, however, well below the 30 year

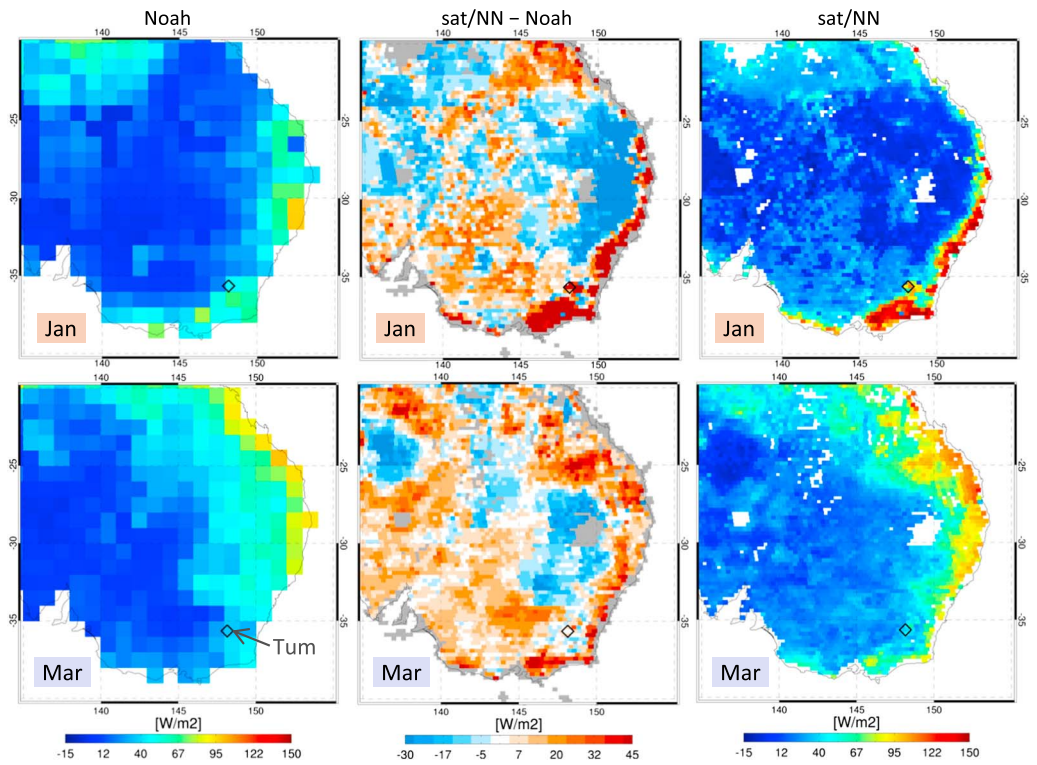


Figure 11. (left) LE from Noah, (right) the satellite/NN product, and (middle) the difference between the two for (top) January and (bottom) March 2003. The FLUXNET site at Tumberumba is marked, near the southeast corner.

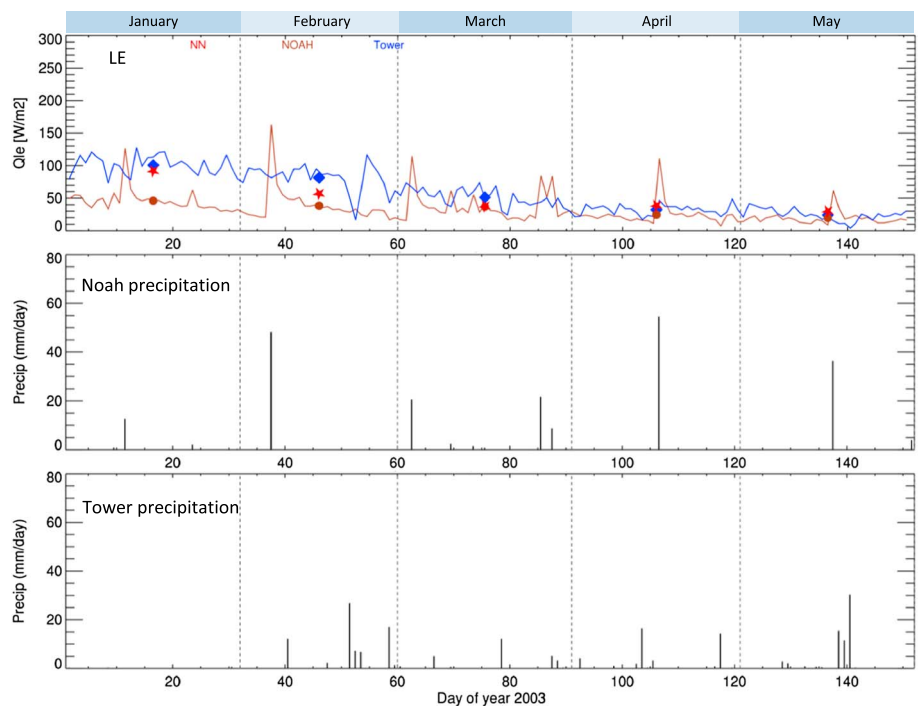


Figure 12. (top) Daily-average LE from Noah (brown), the flux tower (blue), and the satellite/NN (red), and precipitation from (middle) Noah and (bottom) the tower for the Tumberumba site. The markers indicate the monthly averages of LE.

average, and the leaf area was diminished by drought-related insect damage [van Gorsel *et al.*, 2013]. The trees at this site were nevertheless able to extract water deep within the soil and thus could maintain relatively high transpiration (and LE) over this dry period, even as the carbon flux was highly anomalous [Leuning *et al.*, 2005; van Gorsel *et al.*, 2013].

The analyses at the Tumbarumba site have significant similarities to the findings at the Tonzi and Blodgett sites in California (section 4.2). Here also the Noah simulation is hindered by inaccuracies in the precipitation and by inability of the model to represent the forest transpiration over dry periods.

5. Conclusion

Estimates of latent heat flux (LE) derived from microwave, infrared, and visible satellite data products using a neural network were found to have broad similarities and distinct differences when compared with LE estimates derived from other sources. We focused particularly on comparisons between our satellite-derived LE and LE from the Noah land surface model. In several regions with extensive LE discrepancies that persisted for 2 months or more, data from flux towers elucidated the sources of the discrepancies. The primary conclusions of the comparisons and analyses were as follows:

1. LE from our satellite-driven neural network analysis was generally more similar to an analysis generated by upscaling FLUXNET tower data than to LE from the land surface model, despite use of the model LE to train the neural network and the independence of our method from the data used in the upscaled LE.
2. Analysis of data from the Central Great Plains and of land surface model formulations indicated potential problems with the modeled roughness length and turbulent exchange coefficients for midlatitude cropland areas in summer.
3. Inaccuracies in the precipitation data that were used as forcing for the land surface model contributed to LE discrepancies in areas of Northern California and Southeast Australia where water availability was a major control on LE.
4. In forested areas of Northern California and Southeast Australia, the land surface model did not adequately represent the degree to which transpiration by trees maintains elevated LE in dry summer months.
5. The results presented here demonstrate the usefulness of analyzing land surface model data in conjunction with satellite-derived products and flux tower data for identifying circumstances where the land surface model system may benefit from further evaluation and improvement.

For the eight tower sites and the periods of time analyzed in this paper, along with several months of data from four tower sites not presented here (one in Maine and three in the Northern Great Plains), there was generally greater agreement in monthly-average LE between the satellite product and the tower data than there was between the land surface model and the tower data. Mean, RMS, and maximum differences were, respectively, 21, 25, and 60 W/m² for the satellite product and 36, 46, and 147 W/m² for the land surface model. These statistics cannot be considered representative of performance over all land areas or all seasons, since the discrepancies for which we had sufficient tower data were all midlatitude, and snow areas were avoided; nevertheless, these results are encouraging regarding the usefulness of our satellite-derived LE data set for other applications.

References

- Anderson, M. C., J. M. Norman, J. R. Mecikalski, J. A. Otkin, and W. P. Kustas (2007), A climatological study of evapotranspiration and moisture stress across the continental United States based on thermal remote sensing: 1. Model formulation, *J. Geophys. Res.*, *112*, D10117, doi:10.1029/2006JD007506.
- Baldocchi, D. (2003), Assessing the eddy covariance technique for evaluation carbon dioxide exchange rates for ecosystems: Past, present and future, *Global Change Biol.*, *9*, 479–492.
- Baldocchi, D., *et al.* (2001), FLUXNET: A new tool to study the temporal and spatial variability of ecosystem-scale carbon dioxide, water vapor, and energy flux densities, *Bull. Am. Meteorol. Soc.*, *82*, 2415–2434.
- Baldocchi, D. D., L. Xu, and N. Kiang (2004), How plant functional-type, weather, seasonal drought, and soil physical properties alter water and energy fluxes of an oak-grass savanna and an annual grassland, *Agric. For. Meteorol.*, *123*, doi:10.1016/j.agrformet.2003.11.006.
- Berg, A. A., J. Famiglietti, J. Walker, and P. Houser (2003), Impact of bias correction to reanalysis products on simulations of North American soil moisture and hydrological fluxes, *J. Geophys. Res.*, *108*(D16), 4490, doi:10.1029/2002JD003334.
- Bosilovich, M. G., J. D. Radakovich, A. Da Silva, R. Todling, and F. Verter (2007), Skin temperature analysis and bias correction in a coupled land-atmosphere data assimilation system, *J. Meteorol. Soc. Jpn.*, *85A*, 205–228.
- Chen, F., K. Mitchell, J. Schaake, Y. Xue, H.-L. Pan, V. Koren, Q. Y. Duan, M. Ek, and A. Betts (1996), Modeling of land surface evaporation by four schemes and comparison with FIFE observations, *J. Geophys. Res.*, *101*(D3), 7251–7268, doi:10.1029/95JD02165.

Acknowledgments

We thank Hiroko Kato Beaudoin for information and data regarding GLDAS applications of the Noah model and Joe Santanello, Christa Peters-Lidard, David Mocko, Helin Wei, and Michael Ek for information and insight regarding the Noah model formulation and behavior. The GLDAS data used in this study were acquired as part of the mission of NASA's Earth Science Division and were archived and distributed by the Goddard Earth Sciences Data and Information Services Center. For availability and access to flux tower data and related information, we thank Dennis Baldocchi and the Office of Science and Terrestrial Carbon Program, U.S. Department of Energy (Tonzi ranch and Vaira ranch sites); Allen Goldstein (Blodgett forest site); Dave Billesbach, Margaret Torn, and the Office of Science, U.S. Department of Energy (US-ARM site); Tinden Meyers and NOAA/ARL (Bondville site); S. B. Verma and Andy Suyker (Mead, Nebraska site); Richard Counter and David Cook (Walnut River Watershed site); and Eva van Gorsel (Tumbarumba site). FLUXNET and Ameriflux data were obtained from the Oak Ridge National Laboratory Distributed Active Archive Center (<http://fluxnet.ornl.gov> and <http://ameriflux.ornl.gov/>). Marcus Reichstein is thanked for providing data from the LE analysis derived from upscaled FLUXNET data. Data used to produce the results of this paper are available through the Environmental Monitoring section at www.aer.com. The material in this paper is based upon work supported by NASA under award NNX09AK04G.

- Diak, G. R. (1990), Evaluation of heat flux, moisture flux and aerodynamic roughness at the land surface from knowledge of the PBL height and satellite-derived skin temperatures, *Agric. For. Meteorol.*, *52*, 181–198.
- Ek, M. B., K. E. Mitchell, Y. Lin, E. Rodgers, P. Grunman, V. Koren, G. Gayno, and J. D. Tarpley (2003), Implementation of Noah land surface model advances in the National Centers for Environmental Prediction operational mesoscale Eta model, *J. Geophys. Res.*, *108*(D22), 8851, doi:10.1029/2002JD003296.
- Ferrazzoli, P. S., P. Paloscia, G. Pampaloni, D. S. Schiavon, and P. Coppo (1992), Sensitivity of microwave measurements to vegetation biomass and soil moisture content: A case study, *IEEE Trans. Geosci. Remote Sens.*, *30*, 750–756, doi:10.1109/36.158869.
- Fisher, J. B., K. P. Tu, and D. D. Baldocchi (2008), Global estimates of the land-atmosphere water flux based on monthly AVHRR and ISLSCP-II data, validated at 16 FLUXNET sites, *Remote Sens. Environ.*, *112*, 901–919, doi:10.1016/j.rse.2007.06.025.
- Galantowicz, J. F., J.-L. Moncet, P. Liang, A. E. Lipton, G. Uymin, C. Prigent, and C. Grassotti (2011), Subsurface emission effects in AMSR-E measurements: Implications for land surface microwave emissivity retrieval, *J. Geophys. Res.*, *116*, D17105, doi:10.1029/2010JD015431.
- Goldstein, A. H., N. E. Hultman, J. M. Fracheboud, M. R. Bauer, J. A. Panek, M. Xu, Y. Qi, A. B. Guenther, and W. Baugh (2000), Effects of climate variability on the carbon dioxide, water, and sensible heat fluxes above a ponderosa pine plantation in the Sierra Nevada (CA), *Agric. For. Meteorol.*, *101*, 113–129.
- Huete, A., C. Justice, and W. van Leeuwen (1999), MODIS Vegetation Index (MOD 13) Algorithm Theoretical Basis Document, Ver. 3. [Available at http://modis.gsfc.nasa.gov/data/atbd/atbd_mod13.pdf.]
- Jiménez, C., C. Prigent, and F. Aires (2009), Toward an estimation of global land surface heat fluxes from multisatellite observations, *J. Geophys. Res.*, *114*, D06305, doi:10.1029/2008JD011392.
- Jiménez, C., et al. (2011), Global intercomparison of 12 land surface heat flux estimates, *J. Geophys. Res.*, *116*, D02102, doi:10.1029/2010JD014545.
- Jung, M., et al. (2011), Global patterns of land-atmosphere fluxes of carbon dioxide, latent heat, and sensible heat derived from eddy covariance, satellite, and meteorological observations, *J. Geophys. Res.*, *116*, G00J07, doi:10.1029/2010JG001566.
- Kalnay, E., M. Kanamitsu, and W. E. Baker (1990), Global numerical weather prediction at the National Meteorological Center, *Bull. Am. Meteorol. Soc.*, *71*, 1410–1428.
- Kanamitsu, M. (1989), Description of the NMC global data assimilation and forecast system, *Weather Forecasting*, *4*, 335–342.
- Leuning, R., H. A. Cleugh, S. J. Zegelin, and D. Hughes (2005), Carbon and water fluxes over a temperate eucalyptus forest and a tropical wet/dry savanna in Australia: Measurements and comparison with MODIS remote sensing estimates, *Agric. For. Meteorol.*, *129*, 151–173, doi:10.1016/j.agrformet.2004.12.004.
- Li, F., W. P. Kustas, M. C. Anderson, J. H. Prueger, and R. L. Scott (2008), Effect of remote sensing spatial resolution on interpreting tower-based flux observations, *Remote Sens. Environ.*, *112*, 337–349, doi:10.1016/j.rse.2006.11.032.
- Liebe, H. J., P. W. Rosenkranz, and G. A. Hufford (1992), Atmospheric 60-GHz oxygen spectrum: New laboratory measurements and line parameters, *J. Quant. Spectrosc. Radiat. Transfer*, *48*, 629–643.
- Lu, X., and Q. Zhuang (2010), Evaluating evapotranspiration and water-use efficiency of terrestrial ecosystems in the conterminous United States using MODIS and AmeriFlux data, *Remote Sens. Environ.*, *114*, 1924–1939, doi:10.1016/j.rse.2010.04.001.
- Massman, W. J., and X. Lee (2002), Eddy covariance flux corrections and uncertainties in long-term studies of carbon and energy exchanges, *Agric. For. Meteorol.*, *113*, 121–144.
- Mauder, M., and T. Foken (2006), Impact of post-field data processing on eddy covariance flux estimates and energy balance closure, *Meteorol. Z.*, *15*(6), 597–609, doi:10.1127/0941-2948/2006/0167.
- Mauder, M., R. L. Desjardins, E. Pattey, and D. Worth (2010), An attempt to close the surface energy balance using spatially-averaged flux measurements, *Boundary-Layer Meteorol.*, *136*, 175–191, doi:10.1007/s10546-010-9497-9.
- Miralles, D. G., R. R. H. Holmes, R. A. M. De Jeu, J. H. Gash, A. G. C. A. Meesters, and A. J. Dolman (2011), Global land-surface evaporation estimated from satellite-based observations, *Hydrol. Earth Syst. Sci.*, *15*, 453–469, doi:10.5194/hess-15-453-2011.
- Mitchell, K. E., et al. (2004), The multi-institution North American Land Data Assimilation System (NLDAS): Utilizing multiple GCIIP products and partners in a continental distributed hydrological modeling system, *J. Geophys. Res.*, *109*, D07590, doi:10.1029/2003JD003823.
- Moffat, A. M., et al. (2007), Comprehensive comparison of gap-filling techniques for eddy covariance net carbon fluxes, *Agric. For. Meteorol.*, *147*, 209–232, doi:10.1016/j.agrformet.2007.08.011.
- Moncet, J.-L., P. Liang, J. F. Galantowicz, A. E. Lipton, G. Uymin, C. Prigent, and C. Grassotti (2011), Land surface microwave emissivities derived from AMSR-E and MODIS measurements with advanced quality control, *J. Geophys. Res.*, *116*, D16104, doi:10.1029/2010JD015429.
- Monteith, J. L. (1965), Evaporation and environment, *Symp. Soc. Exp. Biol.*, *19*, 205–234.
- Mu, Q., M. Zhao, and S. W. Running (2011), Improvements to a MODIS global terrestrial evapotranspiration algorithm, *Remote Sens. Environ.*, *115*, 1781–1800, doi:10.1016/j.rse.2011.02.019.
- Mu, Q., M. Zhao, and S. W. Running (2013), Algorithm Theoretical Basis Document: MODIS Global Terrestrial Evapotranspiration (ET) Product (NASA MOD16A2/A3) Collection 5, NASA Headquarters, 55 pp. [Available at https://secure.ntsg.umd.edu/publications/2013/MZR13/MOD16_ATBD.pdf.]
- Ocheltree, T. W., and H. W. Loescher (2007), Design of the AmeriFlux portable eddy covariance system and uncertainty analysis of carbon measurements, *J. Atmos. Oceanic Technol.*, *24*, 1389–1406, doi:10.1175/JTECH2064.1.
- Peters-Lidard, C. D., S. V. Kumar, D. M. Mocko, and Y. Tian (2011), Estimating evapotranspiration with land data assimilation systems, *Hydrol. Processes*, *25*, 3979–3992, doi:10.1002/hyp.8387.
- Price, J. C. (1980), The potential for remotely sensed thermal infrared data to infer surface soil moisture and evaporation, *Water Resour. Res.*, *16*, 787–795.
- Prigent, C., F. Aires, W. Rossow, and E. Matthews (2001), Joint characterization of vegetation by satellite observations from visible to microwave wavelengths: A sensitivity analysis, *J. Geophys. Res.*, *106*(D18), 20,665–20,685, doi:10.1029/2000JD900801.
- Reichle, R. H., J. P. Walker, R. D. Koster, and P. R. Houser (2002), Extended versus ensemble Kalman filtering for land data assimilation, *J. Hydrometeorol.*, *3*, 728–740.
- Reichle, R. H., R. D. Koster, J. Dong, and A. A. Berg (2004), Global soil moisture from satellite observations, land surface models, and ground data: Implications for data assimilation, *J. Hydrometeorol.*, *5*, 430–442.
- Reichle, R. H., R. D. Koster, P. Liu, S. P. P. Mahanama, E. G. Njoku, and M. Owe (2007), Comparison and assimilation of global soil moisture retrievals from the Advanced Microwave Scanning Radiometer for the Earth Observing System (AMSR-E) and the Scanning Multichannel Microwave Radiometer (SMMR), *J. Geophys. Res.*, *112*, D09108, doi:10.1029/2006JD008033.
- Rodell, M., et al. (2004), The global land data assimilation system, *Bull. Am. Meteorol. Soc.*, *85*, 381–394.
- Rosenkranz, P. W. (1998), Water vapor microwave continuum absorption: A comparison of measurements and models, *Radio Sci.*, *33*, 919–928, doi:10.1029/98RS01182.

- Ryu, Y., et al. (2011), Integration of MODIS land and atmosphere products with a coupled-process model to estimate gross primary productivity and evapotranspiration from 1 km to global scales, *Global Biogeochem. Cycles*, *25*, GB4017, doi:10.1029/2011GB004053.
- Sheffield, J., G. Goteti, and E. F. Wood (2006), Development of a 50-year high-resolution global dataset of meteorological forcings for land surface modeling, *J. Clim.*, *19*, 3088–3111, doi:10.1175/JCLI3790.1.
- Stisen, S., I. Sandholt, A. Nørgaard, R. Fensholt, and K. Høgh Jensen (2008), Combining the triangle method with thermal inertia to estimate regional evapotranspiration—Applied to MSG-SEVERI data in the Senegal River basin, *Remote Sens. Environ.*, *112*, 1242–1255.
- Sun, J., G. D. Salvucci, and D. Entekhabi (2012), Estimates of evapotranspiration from MODIS and AMSR-E land surface temperature and moisture over the Southern Great Plains, *Remote Sens. Environ.*, *127*, 44–59, doi:10.1016/j.rse.2012.08.020.
- Suyker, A. E., and S. B. Verma (2009), Evapotranspiration of irrigated and rainfed maize-soybean cropping systems, *Agric. For. Meteorol.*, *149*, 443–452.
- Tang, R., Z.-L. Li, and B. Tang (2010), An application of the Ts-VI triangle method with enhanced edges determination for evapotranspiration estimation from MODIS data in arid and semi-arid regions: Implementation and validation, *Remote Sens. Environ.*, *114*, 540–551, doi:10.1016/j.rse.2009.10.012.
- van Gorsel, E., et al. (2013), Primary and secondary effects of climate variability on net ecosystem carbon exchange in an evergreen Eucalyptus forest, *Agric. For. Meteorol.*, *182–183*, 248–256, doi:10.1016/j.agrformet.2013.04.027.
- Venturini, V., S. Islam, and L. Rodriguez (2008), Estimation of evaporative fraction and evapotranspiration from MODIS products using a complementary based model, *Remote Sens. Environ.*, *112*, 132–141.
- Vinukollu, R. K., E. F. Wood, C. R. Ferguson, and J. B. Fisher (2011), Global estimates of evapotranspiration for climate studies using multi-sensor remote sensing data: Evaluation of three process-based approaches, *Remote Sens. Environ.*, *115*, 801–823, doi:10.1016/j.rse.2010.11.006.
- Vinukollu, R. K., J. Sheffield, E. F. Wood, M. G. Bosilovich, and D. Mocko (2012), Multimodel analysis of energy and water fluxes: Intercomparisons between operational analyses, a land surface model, and remote sensing, *J. Hydrometeorol.*, *13*, 3–26, doi:10.1175/2011JHM1372.1.
- Wang, K., and R. E. Dickinson (2012), A review of global terrestrial evapotranspiration: Observation, modeling, climatology, and climatic variability, *Rev. Geophys.*, *50*, RG2005, doi:10.1029/2011RG000373.
- Wang, K., Z. Li, and M. Cribb (2006), Estimation of evaporative fraction from a combination of day and night land surface temperatures and NDVI: A new method to determine the Priestley-Taylor parameter, *Remote Sens. Environ.*, *102*, 292–305, doi:10.1016/j.rse.2006.02.007.
- Zhang, Y., W. Rossow, A. Lacis, V. Oinas, and M. Mishchenko (2004), Calculation of radiative fluxes from the surface to top of atmosphere based on ISCCP and other global data sets: Refinements of the radiative transfer model and the input data, *J. Geophys. Res.*, *109*, D19015, doi:10.1029/2003JD004457.
- Zheng, W., H. Wei, Z. Wang, X. Zeng, J. Meng, M. Ek, K. Mitchell, and J. Derber (2012), Improvement of daytime land surface skin temperature over arid regions in the NCEP GFS model and its impact on satellite data assimilation, *J. Geophys. Res.*, *117*, D06117, doi:10.1029/2011JD015901.